Structures of sequential open states in a symmetrical opening transition of the TolC exit duct

Xue-Yuan Pei[1,2], Philip Hinchliffe[1,3], Martyn F. Symmons[4], Eva Koronakis, Roland Benz[5], Colin Hughes, and Vassilis Koronakis

Department of Pathology, Cambridge University, Cambridge CB2 1QP, United Kingdom

Edited* by Tom A. Rapoport, Harvard Medical School/HHMI, Boston, MA, and approved December 16, 2010 (received for review August 25, 2010)

In bacterial drug resistance and virulence pumps, an inner membrane (IM) transporter and periplasmic adaptor recruit an outer membrane (OM) trimeric TolC exit duct that projects an α-helical tunnel across the periplasm. The TolC periplasmic entrance is closed by densely packed α-helical coiled coils, inner H7/H8, and outer H3/H4, constrained by a hydrogen bond network. On recruitment, these coiled coils must undergo transition to the open state. We present 2.9 Å resolution crystal structures of two sequential TolC open states in which the network is incrementally disrupted and channel conductances defined in lipid bilayers. Superimposition of TolC^{RS} (370 pS) and TolC^{YFRS} (1,000 pS) on the TolC^{WT} closed state (80 pS) showed that in the initial open-state TolC^{RS}, relaxation already causes approximately 14° twisting and expansion of helix H7 at the periplasmic tip, increasing interprotomer distances from 12.2 Å in TolC^{WT} to 18.9 Å. However, in the crystal structure, the weakened Asp^{374} pore constriction was maintained at the closed state 11.3 Å^2. In the advanced open-state TolC^{YFRS}, there was little further expansion at the tip, to interprotomer 21.3 Å, but substantial movement of inner and outer coiled coils dilated the pore constriction. In particular, upon abolition of the TolC^{YFRS} intraprotomer Tyr^{362}–Asp^{153} link, a redirection of Tyr^{362} and "bulge" in H3 allowed a simple movement outward of H8, establishing a 50.3 Å^2 opening. Root mean square deviations (rmsds) over the coiled coils of the three protomers of TolC^{RS} and TolC^{YFRS} illustrate that, whereas independent movement at the periplasmic tips may feature in the initial stages of opening, full dilation of the pore constriction is entirely symmetrical.

antibiotic resistance | drug efflux | type I export | X-ray crystal structure

Gram-negative bacteria such as *Escherichia coli*, *Salmonella enterica*, and *Pseudomonas aeruginosa* have inner and outer cell membranes separated by the periplasmic space. To expel diverse antibiotics and other noxious chemicals and to export large protein toxins (1–3), bacteria use tripartite machineries, or pumps, that span the entire cell envelope (4). These pumps are important to survival, especially in infections where they contribute to multidrug resistance and virulence.

In assembled pumps, an inner membrane (IM) transporter, typically a proton antiporter (drug efflux) or ATPase (protein export), interacts with a periplasmic adaptor protein. This complex recruits a TolC exit duct, which is anchored in the outer membrane (OM) and projects across the periplasm. The structures of all three drug efflux pump components are known: the trimeric TolC exit duct (5), the trimeric AcrB transporter (6, 7), the partial adaptor AcrA (8), and the complete homologous *Pseudomonas* adaptor MexA (9, 10). We have established a model of the assembled tripartite machinery on the basis of extensive site-specific cross-linking between the flexible, linearly arranged multidomain adaptor and its two cognate partner proteins (9, 11). To recruit TolC, the 47 Å long α-hairpin domain of the adaptor packs against intramolecular grooves formed by entrance helices of each TolC protomer (9, 11). Several domains of the adaptor bind to the IM transporter AcrB, while the TolC entrance helices make tip-to-tip contacts with AcrB (12, 13). The assembly is stabilized by a single adaptor on each subunit, sealing the assembled pump against the periplasm (9).

Trimeric TolC is a 12-stranded α/β-barrel (Fig. 1*A*), a unique structure that presents a single pore through an OM β-barrel and a contiguous 100 Å long α-helical tunnel through the periplasm (5). In the resting state, the periplasmic entrance of TolC is closed to substrates as three of the six pairs of 2-stranded coiled coils, one from each 471-residue protomer, fold inward (the inner coils). In particular, a ring of Asp^{371} and Asp^{374} residues form the narrowest pore constriction (Fig. 1*B*, cross-section 1). At the tip of the periplasmic entrance (Fig. 1*B*, cross-section 3), where TolC interacts with the apex of AcrB, the coiled coils are relatively unconstricted with the connecting turns of the inner and outer helix pairs exposed.

To allow drug efflux and protein export, the TolC periplasmic entrance must be opened. The proposed allosteric opening mechanism (5) envisages that the inner coiled-coil α-helices (H7/H8) undergo an iris-like movement to realign with the outer coils (H3/H4), thereby enlarging the pore in a "twist-to-open" transition (5, 14). This hypothesis is supported by locking (cross-linking) the entrance coils in a closed state in vivo, which disables export of substrates engaged in the assembled pump (15), and by comparative planar lipid bilayer conductance measurements of TolC variants in which links constraining the coiled coils of the resting state were severed incrementally (14). The network of constraining hydrogen bonds centers on four key residues: Thr^{152}, Asp^{153}, Tyr^{362}, and Arg^{367} (Fig. 1*B*, cross-section 2). The intraprotomer bond Tyr^{362}–Asp^{153} tethers the inner coiled-coil H7/H8 to the outer coiled-coil H3/H4, while simultaneously the interprotomer bonds, Arg^{367}–Asp^{153} and Arg^{367}–Thr^{152}, link helix H8 to H4. Substitution of R^{367}S gave a conductance of 205–370 pS (TolC^{RS}), a 2- to 4-fold increase over the "closed" TolC^{WT} (80 pS). Simultaneous substitution of Y^{362}F and R^{367}S (TolC^{YFRS}) caused a 10- to 12-fold conductance increase, from 80 pS (TolC^{WT}) to a maximum conductance of 800–1,000 pS, suggesting an open state sufficient to allow exit of diverse substrates.

Understanding the TolC opening mechanism requires precise views of the structural changes underlying recruitment and

Author contributions: P.H., C.H., and V.K. designed research; X.-Y.P., P.H., M.F.S., E.K., and R.B. performed research; X.-Y.P., P.H., M.F.S., E.K., R.B., C.H., and V.K. analyzed data; and P.H., M.F.S., E.K., C.H., and V.K. wrote the paper.

The authors declare no conflict of interest.

*This Direct Submission article had a prearranged editor.

Data deposition: The atomic coordinates and structure factors have been deposited in the Protein Data Bank, www.pdb.org [PDB ID codes 2WMZ (TolC^{RS}) and 2XMN (TolC^{YFRS})].

[1]X.-Y.P. and P.H. contributed equally to this work.

[2]Present address: Department of Biochemistry, Cambridge University, 80 Tennis Court Road, Cambridge CB2 1GA, United Kingdom.

[3]To whom correspondence should be addressed. E-mail: ph298@cam.ac.uk.

[4]Present address: European Bioinformatics Institute, Wellcome Trust Genome Campus, Hinxton, Cambridge CB10 1SD, United Kingdom.

[5]Present address: School of Engineering and Science, Jacobs University Bremen, 28759 Bremen, Germany.

This article contains supporting information online at www.pnas.org/lookup/suppl/doi:10.1073/pnas.1012588108/-/DCSupplemental.

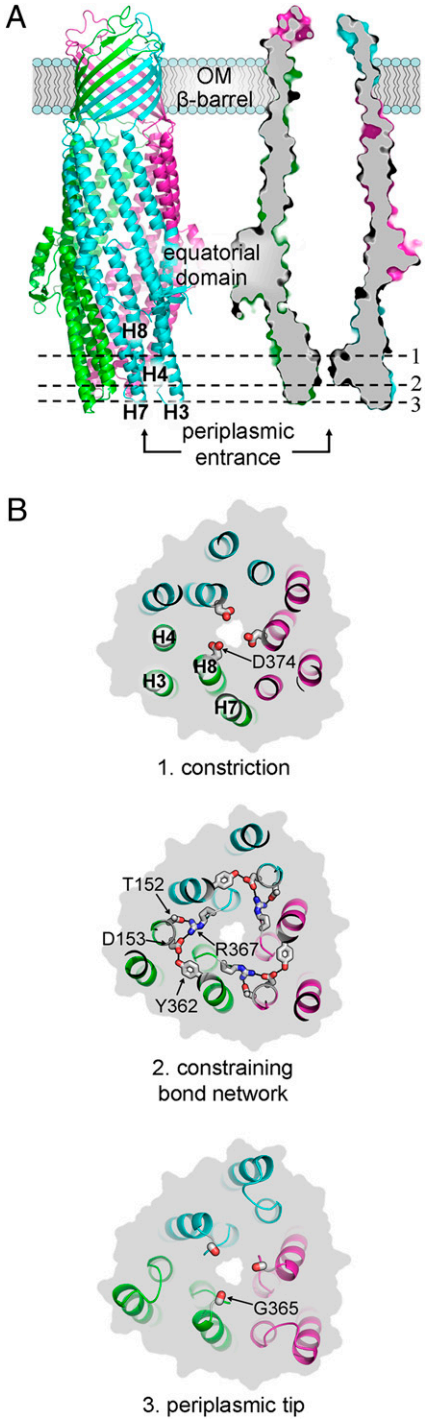

Fig. 1. Structural overview of the TolC periplasmic entrance. (*A*) Side view of the resting closed state of trimeric TolC. (*Left*) The three protomers colored green, blue, and magenta. H3, H4, H7, and H8 are the periplasmic α-helices that rearrange during the opening of TolC (5, 14). (*Right*) A slice through a space-filling model of the TolC trimer, showing the contiguous pore from the outer membrane (OM) β-barrel to the equatorial domain and the α-barrel periplasmic entrance. Dashed lines indicate cross-sections through TolC, at the levels of the following: 1, the Asp^{374} ring constriction; 2, the constraining bond network; and 3, the periplasmic tip. (*B*) Cross-sections indicated by dashed lines in *A*, viewed through the pore toward the equatorial domain and OM β-barrel. The gray background outlines the surface representation. 1, the narrowest constriction of the pore formed by a ring of Asp^{374} residues (5). 2, the constraining bond network of the periplasmic entrance coils showing the residues central to the key intra- and interprotomer links identified as stabilizing the resting closed state (14). R^{367} forms

transition of the coiled coils to the open state. Here, we provide 2.9 Å structures of two biophysically defined TolC open states, $TolC^{RS}$ and $TolC^{YFRS}$, which present sequential snapshots of the transition to advanced opening.

Results

The TolC variants $TolC^{RS}$ (370 pS) and $TolC^{YFRS}$ (1,000 pS) were crystallized and structures solved at 2.9 Å resolution in the space group $P2_12_12_1$. Their crystallographic data are summarized in Table S1. In $TolC^{RS}$ the interprotomer bonds Arg^{367}–Asp^{153} and Arg^{367}–Thr^{152} are disrupted, whereas in $TolC^{YFRS}$, the intraprotomer link Tyr^{362}–Asp^{153} is also lost. Both structures show large rearrangements of the periplasmic entrance coiled coils. In $TolC^{RS}$, changes are evident from around Ser^{353} (on inner helix H7), approxmately 18 Å from the periplasmic tip, whereas in $TolC^{YFRS}$, realignment begins on the same helix around Gln^{342}, approximately 35 Å from the tip. In neither are there significant changes in the equatorial domain or above in the α/β-barrel, reflected in their considerably lower B factors relative to the rest of the two structures (main chain and side chain 15–17% less than average). The key aspects of the structural changes underlying opening are analyzed by viewing three cross-sections of the periplasmic entrance domain (Fig. 1), namely the constraining bond network (cross-section 2), the Asp^{374} pore constriction (cross-section 1), and the periplasmic tip (cross-section 3) after superimposing invariant domains of each of the open-state structures on those of $TolC^{WT}$.

Structural Rearrangements in the Constraining Bond Network. The rearrangements of the entrance helices in the crystal structures of $TolC^{RS}$ and $TolC^{YFRS}$ are shown in Fig. 2. Abolition of the interprotomer Arg^{367} bonds in $TolC^{RS}$ permits a large outward realignment of the inner coiled-coil helix H7, without affecting a more static inner helix H8 [illustrated by superimposition of $TolC^{WT}$ (blue) with $TolC^{RS}$ (red) in Fig. 2*A*]. This is likely to reflect the intraprotomer H bond between Tyr^{362} and Asp^{153} remaining intact due to a significant rotameric rearrangement of the Tyr^{362} side chain (Fig. 2*A*, *Upper*); both in the resting closed state ($TolC^{WT}$) and the lower conductance open state ($TolC^{RS}$) residue Tyr^{362} blocks any movement outward of H8. This is further evident in the advanced open-state $TolC^{YFRS}$, in which abolishing the Tyr^{362}–Asp^{153} intraprotomer bond allows the side chain of Tyr^{362} to be redirected outward away from H4 in the outer coiled coils (Fig. 2*A*, *Lower*, $TolC^{WT}$ superimposed with $TolC^{YFRS}$ in green). This redirection is significant in allowing space for H8 to move outward (Fig. 2*B*) which, as will be detailed in the following section, is necessary to dilate the pore. Although Asp^{153} and Thr^{152} on H4 are no longer bonded to H8, there is little movement of these residues, apart from a very slight anticlockwise twist.

Dilation of the Pore Constriction at the Asp^{374} Ring. For drugs and proteins to be expelled by TolC, relaxation of the constraints (Fig. 1, cross-section 2) must translate to dilating the Asp^{374} constriction (Fig. 1, cross-section 1). Nonetheless, the $TolC^{RS}$ structure shows that the substantial changes in the constraining bond network have not translated to an increase in the TolC aperture (Fig. 3*A*, $TolC^{RS}$ pore in red). In fact, in the $TolC^{RS}$ crystal structure, the pore appears closed like $TolC^{WT}$ (Fig. 3*B*, *Left*), with the same cross-sectional area of 11.3 $Å^2$ (calculated with the program, HOLE; ref. 16). The closed state is sustained despite a slight,

interprotomer bonds with both T^{152} and D^{153}, whereas Y^{362} forms an intraprotomer bond with D^{153}. 3, the periplasmic tip of the entrance coils at the level of Gly^{365}, which lies on the connecting loop of the inner coiled coil (H7 to H8).

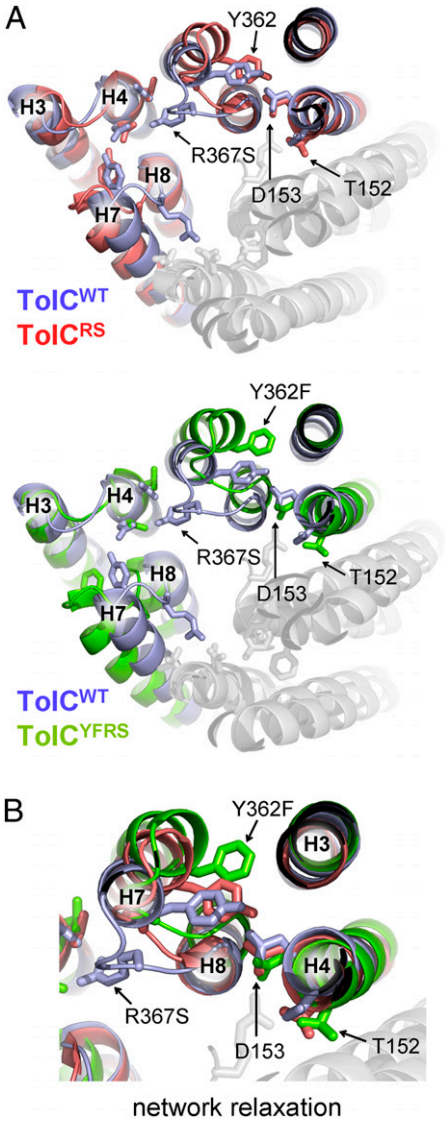

Fig. 2. Relaxation of the constraining network in the open-state crystal structures. Superimpositions of TolC^{WT} (blue) with TolC^{RS} (red) and TolC^{YFRS} (green) based on invariant sections, showing structural rearrangements around the mutated residues R^{367}S and Y^{362}F, which in the wild type, form constraining hydrogen bonds (to D^{153} and T^{152}) at the periplasmic entrance (Fig. 1, cross-section 2). To allow a clearer view of the side chain movements, TolC is tilted. (*A*, *Upper*) Superimposition of TolC^{WT} (blue) with TolC^{RS} (red). (*Lower*) Superimposition of TolC^{WT} (blue) with TolC^{YFRS} (green). Two protomers from each open state are shown, with the inner (H3/H4) and outer (H7/H8) coiled-coil α-helices indicated on one protomer. The residues that form constraining bonds are labeled in the second protomer. The third protomer is shown in gray. (*B*) Cumulative rearrangements of the constraining bond network, shown as side chains and helices in a single protomer of TolC^{WT}, TolC^{RS}, and TolC^{YFRS}.

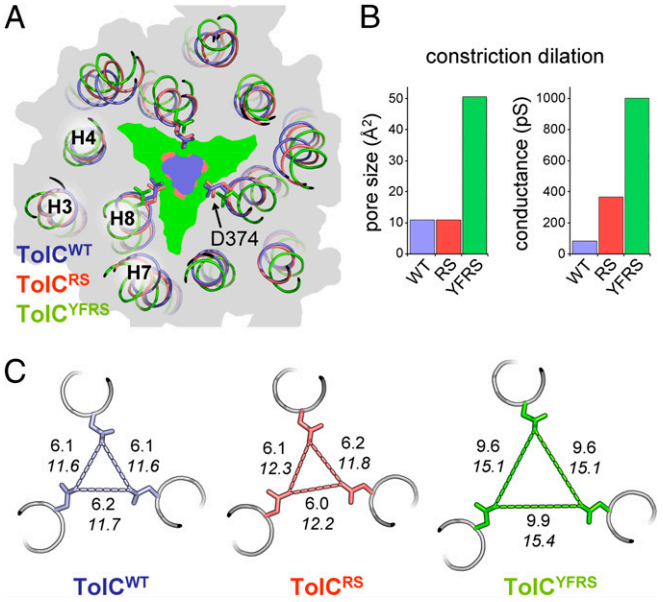

Fig. 3. Dilation of the pore at the Asp^{374} ring constriction. (*A*) Superimposition of TolC^{WT} (blue), TolC^{RS} (red), and TolC^{YFRS} (green) viewed as a slab at the level of the narrowest constriction, formed by the Asp^{374} ring. The gray background outlines the surface representation (of TolC^{YFRS}). (*B*) Pore dilation in the open-state crystal structures and planar lipid bilayers. (*Left*) Surface area of the open-state pores at the narrowest constriction, as shown in *A*. (*Right*) The maximum conductance for each open state (14). (*C*) Distances between Asp^{374} residues of the three TolC protomers in the three states, measured in angstroms between the side chain $O_{\delta 2}$ atoms. The distances between the C_α atoms is given in italics below in each case.

approximately 0.5 Å movement outward of H8 (indicated in Fig. 3*C* by the italicized C_α distances of Asp^{374}) and is due to a rearrangement of the Asp^{374} side chains, which keeps the interprotomer distances between side chain $O_{\delta 2}$ atoms the same as in TolC^{WT} (Fig. 3*C*, TolC^{WT} 6.1–6.2 Å, TolC^{RS} 6.0–6.2 Å). Within H-bonding distance of Asp^{374} on one of the TolC^{RS} protomers is density for a water molecule or metal ion (such as Na^+) that may help to mediate this Asp^{374} side chain rearrangement and thus maintain the constriction. That the TolC^{RS} constriction in the crystal structure is effectively identical to TolC^{WT}, despite its increased conductance from 80 pS to 370 pS (Fig. 3*B*, *Right*), indicates that the Asp^{374} constriction is weakened and can dilate at high ionic strength when high cation flux is applied through the channel in lipid bilayers. In the absence of such forces, the constriction is maintained.

As the opening advances, illustrated by TolC^{YFRS}, the situation is markedly different. The additional disruption of the other key link, intraprotomer Tyr^{362}–Asp^{153}, allows the realignment of the innermost helix H8 and significantly increases the size of the pore at the Asp^{374} constriction (Fig. 3*A*), expanding the 11.3 Å^2 surface area of the resting closed state (TolC^{WT}) to 50.3 Å^2 in TolC^{YFRS} (Fig. 3*B*, *Left*). This is reflected in the interprotomer distances of Asp^{374}, which increase from 6.1–6.2 Å in TolC^{WT} to 9.6–9.9 Å in TolC^{YFRS}. The dilation of the pore constriction is also reflected in the 12-fold increase in conductance of TolC^{YFRS} over TolC^{WT} (Fig. 3*B*, *Right*). Nevertheless, the electrophysiology of TolC^{YFRS} in lipid bilayers indicated that the lifetime of the 1,000 pS open state was short, with frequent switches into lower conductance substates. The stable state presented by the crystal structure of TolC^{YFRS} would therefore not necessarily determine the maximum 1,000 pS shown in Fig. 3*B*, but possibly an intermediate or average conductance state. Notwithstanding, the TolC^{YFRS} structure illustrates clearly the coupled action of inner and outer entrance helices in an advanced stage of opening.

Twist and Expansion of the α-Helices at the Periplasmic Entrance Tip. The exposed periplasmic tips of the TolC entrance (Fig. 1, cross-section 3) interact with the apex of AcrB (9). On disruption of the bond network, in both TolC^{RS} and TolC^{YFRS}, the tips undergo immediate large changes (Fig. 4*A*), highlighted by the movement of Gly^{365} at the very tip of the exposed loop connecting the inner coiled-coil helices H7 and H8 on each of the

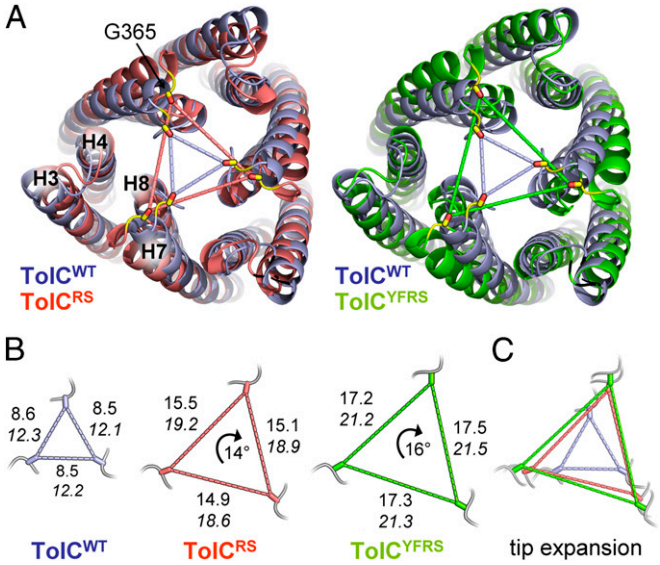

Fig. 4. Helical movements and expansion at the periplasmic tip. (*A*) TolC viewed from the periplasmic entrance toward the equatorial domain and OM β-barrel. Gly^{365} (yellow), situated on the loop connecting inner-helices H7 and H8 at the exposed periplasmic tips of TolC. Distances between Gly^{365} on the protomers are shown. (*Left*) Superimposition of $TolC^{WT}$ (blue) and $TolC^{RS}$ (red). (*Right*) Superimposition of $TolC^{WT}$ (blue) and $TolC^{YFRS}$ (green). (*B*) Distances between Gly^{365} residues of the three protomers for $TolC^{WT}$ (blue), $TolC^{RS}$ (red), and $TolC^{YFRS}$ (green) are indicated by dashed lines and measured in angstroms between the oxygen atoms, with the measurement between the carboxyl carbon atoms beneath in italics. The degree of twisting of Gly^{365}, relative to $TolC^{WT}$, is shown by the arrow in the center of the triangles for $TolC^{RS}$ and $TolC^{YFRS}$. (*C*) Summary of the expansion and twist at the periplasmic tip from $TolC^{WT}$ to both $TolC^{RS}$ and $TolC^{YFRS}$, shown as an overlay of the movements of Gly^{365} in *B*.

three protomers. The movement is both an expansion and a twist.

In $TolC^{RS}$, realignment of Gly^{365} increases the distance between protomer helices to 18.9 Å, from 12.2 Å in $TolC^{WT}$ (Fig. 4*B*). This distance in $TolC^{RS}$ differs by 0.6 Å between the three protomers, suggesting the protomer tips have room for individual movement. In $TolC^{YFRS}$, realignment of Gly^{365} generates a distance of 21.3 Å between protomers, with a variation of only 0.2 Å (Fig. 4*B*). Although these movements of Gly^{365} in $TolC^{YFRS}$ are large compared with the resting closed state of $TolC^{WT}$, they represent a small advance on $TolC^{RS}$ (Fig. 4*C*), only an additional 1.2–1.5 Å. The much higher conductance of $TolC^{YFRS}$ compared with $TolC^{RS}$ is not determined by this small movement, but by the dilation of the pore constriction described in the previous section and Fig. 3. Although in $TolC^{YFRS}$ both H7 and H8 helices realign, the almost identical repositioning of Gly^{365} in $TolC^{RS}$ is caused solely by conformational change of H7, with H8 remaining static. This difference between the two inner helices is permitted without any "stretching" of the loop between them as H7 twists around H8, keeping the connecting loop in the same conformation as in $TolC^{WT}$. Thus, alongside the movement outward of Gly^{365} in both $TolC^{RS}$ and $TolC^{YFRS}$, there are concomitant twists about the pore axis of 14° and 16°, respectively (Fig. 4*B*). The conformational changes at the tips of the inner helices (H7/H8) are not mirrored in the outer helices (H3/H4), which have not moved significantly from the $TolC^{WT}$ position in either $TolC^{RS}$ or $TolC^{YFRS}$. A small 1.3 Å movement inward of H3 in $TolC^{RS}$ is unlikely to be physiologically relevant but may allow the outer helices the flexibility to adapt, if needed, upon AcrB interaction. Even though H3 and H4 do not move at the tip, in $TolC^{YFRS}$ there is a considerable "bulging" outward further along the helices caused by the movement of H8 at the Asp^{374} constriction. This flexibility in the outer coiled coils, in conjunction with the movement of Tyr^{362} (Fig. 2*B*), is essential in allowing space for the realignment of inner helix H8 and thus dilation of the pore aperture.

Discussion

On the basis of stepwise disruption of the entrance-constraining links and characterization of resulting TolC variants in planar lipid bilayers, we proposed an iris-like rearrangement of entrance helices to open the pore constriction (5, 14, 15). We reasoned that a similar realignment would be induced and stabilized in the tripartite pump, by interaction with the IM transporter at the TolC periplasmic tip and by extensive repacking of the TolC entrance helices against the periplasmic adaptor α-hairpin (2, 9, 11).

By elucidating the crystal structures of two different electrophysiologically-defined open states we present sequential snapshots of TolC dilation, as cumulative relaxation of the constraining network allows expansion at both the periplasmic tip and the Asp^{374} pore constriction. In the moderate conductance state of $TolC^{RS}$ (370 pS compared with the 80 pS of $TolC^{WT}$), disruption of the interprotomer Arg^{367} bonds to Asp^{153} and Thr^{152} causes inner helix H7 at the periplasmic tip to undergo a significant twist and expansion around H8. The magnitude of twist and expansion is similar in the advanced open-state $TolC^{YFRS}$ (800–1,000 pS), with interprotomer distances of 18.9 Å ($TolC^{RS}$) and 21.3 Å ($TolC^{YFRS}$). Apparently, therefore, disruption of the interprotomer links is the key to movements at the periplasmic tip. Nonetheless, inner helix H8 is static in $TolC^{RS}$, its movement blocked by rotation of the Tyr^{362} side chain, which retains its intraprotomer interaction with Asp^{153}. In $TolC^{YFRS}$, abolition of this Tyr^{362}–Asp^{153} bond allows a redirection outward of Tyr^{362}, subsequently providing space for the movement of H8. The twist in H7 is not propagated to the Asp^{374} pore constriction, as H8 dilates from the closed/resting state ($TolC^{WT}$) to the early ($TolC^{RS}$) and advanced ($TolC^{YFRS}$) opening states. Thus, whereas the opening features an initial twist of H7 at the periplasmic tip, at the narrowest constriction (cross-section 1, Fig. 1) there is a simple movement outward, or dilation, of H8.

Notwithstanding the significant conformational changes at the periplasmic tip, the $TolC^{RS}$ pore constriction is surprisingly still limited at 11.3 $Å^2$, equal to $TolC^{WT}$ (Fig. 3*A*), restrained at the level of Asp^{374} by the Tyr^{362} side chain and possibly by the solvent molecule apparent in the Asp^{374} ring, similar to the artificially liganded "blocking" cobalt hexamine (17). Opening the pore constriction of $TolC^{YFRS}$ to 50.3 $Å^2$ requires not only the redirection of the Tyr^{362} side chain but also a bulge in outer helix H3 that does not occur in the initial open-state $TolC^{RS}$. These movements of H3, H7, and H8 in $TolC^{YFRS}$ that allow advanced opening of the pore constriction occur at the likely binding site of the adaptor AcrA. Indeed, docking AcrA onto $TolC^{YFRS}$ shows improvement of the already substantial interaction of the 47 Å long AcrA α-hairpin with the $TolC^{WT}$ intraprotomer groove, which we have modeled on the basis of extensive in vivo site-specific crosslinking (11). This is illustrated in Fig. 5*A*, as the AcrA α-hairpin moves from its predocked (gray) to docked (orange) position its interaction is closer with $TolC^{YFRS}$ (green) than with $TolC^{WT}$ (blue), as the H3 and H7 helices move outward. The hinge-like movement between the AcrA lipoyl and α-hairpin domains facilitates this interaction in which the previously established (9, 11) register and structural features of TolC–AcrA docking are retained, i.e., the AcrA α-hairpin forms a pseudodimeric interaction with TolC H3/H4 and a pseudo threefold arrangement at the center of the interaction with the intraprotomer groove formed by outer helices H3/H4 and inner helices H7/H8 (as in refs. 9, 11). Nevertheless, the docking reveals additional space for H8 to dilate further, with a gap between the N-terminal helix of AcrA and H8 of $TolC^{YFRS}$ at the level of the

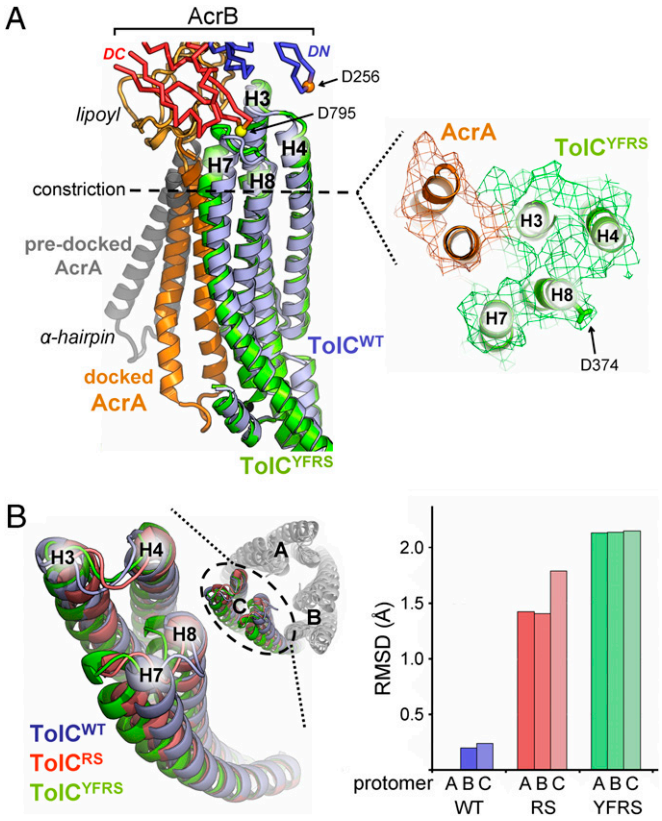

Fig. 5. Symmetry in the TolC advanced open state: enhanced docking to the periplasmic adaptor. (*A*, *Left*) TolC^{YFRS} (green) docked to the periplasmic adaptor AcrA (orange), using established methods (*Materials and Methods*). TolC^{WT} (blue) indicates the movement of TolC^{YFRS} inner (H7/H8) and outer (H3/H4) coils. The crystal structure of AcrA, predocking, is shown in gray and indicates its conformational change relative to the lipoyl domain that is held constant in docking. An "open" model of AcrB (DC domain, red; DN domain, blue) is shown docked to TolC^{YFRS} (*Materials and Methods*), with the C_α atoms of Asp^{256} and Asp^{795} in orange and yellow, respectively. (*Right*) A cross-section through the surface at the level of the Asp^{374} constriction of TolC^{YFRS} (green mesh) with AcrA docked (orange mesh). (*B*, *Left*) structural rearrangements of H3/H4 (outer coils) and H7/H8 (inner coils) viewed in a single protomer (residues 107–186 and 326–405, of the outer and inner coils, respectively) of TolC^{WT} (blue), TolC^{RS} (red), and TolC^{YFRS} (green) superimposed. (*Right*) Rmsds of the coiled coils (over the residues shown *Left*, on H3, H4, H7, and H8) of TolC^{WT} to the respective protomers (chains A, B, and C) of the two open states, TolC^{RS} and TolC^{YFRS}. To determine the rmsds over the coiled coils in TolC^{WT}, protomers B and C were calculated to protomer A.

Asp^{374} constriction (Fig. 5*A*, *Right*). This would allow passage through the pore of pump substrates such as unfolded toxin polypeptide chains and the acridine ring systems of antibiotics, which are approximately 10 Å and 8 Å wide, respectively.

Previously, a 3.2 Å resolution structure of a biophysically uncharacterized TolC form (TolC^{YFRE}) showed modest opening of the constriction (18). The principal conclusion from this partially open structure was that the entrance aperture opens in an asymmetric manner (18), the attraction being that TolC opening would be driven by an asymmetric peristaltic mechanism of the transporter AcrB (19, 20). This conclusion was based on TolC^{YFRE} crystal structures solved either at nonphysiological pH 10.5 (in bilayers varying pH has substantial effects on TolC channel behavior; ref. 21) or in a space group (C2) in which the entrances of two TolC trimers are sterically hindered in the crystal, apparently imposing asymmetry and inhibiting the key movements of the coiled coils that we observe in TolC^{RS} and TolC^{YFRS}. For example, the important bulge of outer coil H3 in the advanced open-state TolC^{YFRS} was not apparent in TolC^{YFRE}, in which it was suggested that inner helices H7 and H8 swing around "stator"-like outer helices H3 and H4 (18). The movement of H3 in the symmetric TolC^{YFRS} precludes the widening of the AcrA-binding intraprotomer groove suggested by the purported asymmetric opening (18). Significantly, these key transitions of the coiled coils in TolC^{YFRS} determine an improved interaction of AcrA with TolC^{YFRS}, illustrated by an enhancement of the theoretical binding energy (as estimated by the docking program Hex, ref. 22), which is approximately 25% greater than that obtained for AcrA docking to the partially open TolC^{YFRE}. For the asymmetry proposed in the AcrB peristaltic mechanism to perpetuate to TolC during pump function, the adaptor would have to transmit conformational changes in individual AcrB protomers to individual TolC protomers, which in turn would depend on the adaptor contacting the AcrB subdomains (localized around PC2) that undergo these conformational changes (19, 20). This is incompatible with our data-based modeling, which shows that the adaptor binds well away from this AcrB region, on the relatively conformationally stable surfaces of the PN2, PC1, DN, and DC AcrB subdomains (9). AcrB itself contacts the TolC entrance as a trimer, with the DN and DC subdomains engaging the three TolC protomers simultaneously. However, as AcrB conformational changes do not involve DN and DC (19, 20), even if TolC entrance tips can move individually, symmetry would likely be imposed on them during AcrB engagement.

The 2.9 Å crystal structures of TolC^{RS} and TolC^{YFRS} sequential open states, defined by electrophysiology and crystallography at physiological pH, also argue against the notion of an asymmetrically open pore constriction. Fig. 5*B*, *Left* summarizes the movements of the entrance helices in a single protomer of TolC^{WT}, TolC^{RS}, and TolC^{YFRS}. Fig. 5*B*, *Right* shows the root mean square deviation (rmsd) differences between these helices in the three protomers of the three crystal structures. These reveal slight asymmetry in the TolC^{RS} early open state [similar to TolC^{YFRE} crystallized in the same space group and cell dimensions ($P2_12_12_1$; $a = 128.28$, $b = 136.18$, $c = 136.13$)]. Importantly, in TolC^{RS}, this affects only the tips of the entrance coils, not the pore constriction. In the advanced open state of TolC^{YFRS}, there are no significant differences between the three protomers, i.e., there is no asymmetry in the tips or pore constriction. Whereas independent protomer movement at the periplasmic tips might therefore be a feature of the initial stages of opening, full dilation of the pore constriction is entirely symmetrical.

Notwithstanding the above, we have nevertheless sought to determine whether there is evidence for asymmetric states of TolC. First, we set out to capture in vivo any stable or transient dimeric intermediates that would be characteristic of an asymmetric opening (Fig. S1). The experiment, which allowed interprotomer disulfide bridges to form in TolC cysteine mutants, captured 100% trimers and monomers, but no asymmetric dimer intermediates. We also looked at the distribution of conductances of TolC^{YFRS} and TolC^{YFRE} channels at physiological pH in lipid bilayers (Fig. S2). These were identical with no evidence of stable, major substates, suggesting that the asymmetrical, smaller pore constriction of TolC^{YFRE}, visualized at pH 10.5, is not physiologically relevant. Finally, as we could not find evidence for asymmetric open states, we forced the TolC pore constriction into an asymmetric state by chemical cross-linking in vivo. This showed (Fig. S3) that an asymmetric TolC entrance does not allow passage of export substrate engaged at the assembled pump. These experiments further support an opening mechanism in which the three TolC protomers dilate to fully open the single central pore in a threefold symmetrical arrangement.

As we have shown in our data-based model (9), pump assembly results in a close AcrB–TolC tip-to-tip fit (Fig. 5*A*), where the exposed, unconstrained loops of the TolC H3/H4 and H7/H8 coiled coils nestle between the two β-hairpins of the AcrB N- and C-terminal docking domains (DN and DC, respectively). In par-

ticular, residue Asp^{256} (on DN) aligns in the $TolC^{YFRS}$ interprotomer gap, the register established (9) in our model of the pump assembly [which is incompatible with the prediction (12, 18) that residue DC-Asp^{795} aligns in the TolC interprotomer gap]. It is possible therefore that Asp^{256} would interrupt the TolC interprotomer Arg^{367}–Asp^{153} link, initiating expansion of the periplasmic tip. In addition, Asp^{795} (or possibly Gln^{797} on the same loop) is well placed to make contact with Tyr^{362} as it redirects outward in the advanced open-state $TolC^{YFRS}$, potentially stabilizing this movement. The ability of the coiled coils in $TolC^{RS}$ to change so significantly at their tips without opening the constriction strengthens the view that assembly of the tripartite machinery can begin without opening the TolC exit duct, and that more than tip-to-tip interaction with AcrB is required to fully open TolC. It follows that TolC interaction with the AcrA adaptor is required to induce and/or stabilize transition to a fully open channel.

Materials and Methods

Protein Purification and Crystallization. $TolC^{RS}$ and $TolC^{YFRS}$ (14) were overexpressed in $TolC^{-}$ *Escherichia coli* (4) and purified, essentially as previously the wild-type TolC (21). Briefly, membranes were solubilized in 5% Triton X-100 from which proteins were purified by Q-sepharose ion-exchange chromatography. TolC fractions were precipitated by isopropanol, the nonessential 43 C-terminal residues removed with V8 protease (5), and the proteins precipitated with a 30–40% PEG 2000 MME/PEG 400 mixture and pelleted at 120,000 *g*. The $TolC^{RS}$ pellet was resuspended in buffer A [0.15% dodecyl maltoside (DDM), 20 mM Tris pH 8.0, 100 mM NaCl] and $TolC^{YFRS}$ in buffer B (0.15% DDM, 20 mM Tris pH 7.5). Crystallization was by vapor diffusion, where 0.5 μL $TolC^{RS}$ protein (15 mg/mL buffer A + 0.6% octylglucoside) was mixed with 0.5 μL reservoir (50 mM Tris pH 8.0, 50 mM NaCl, 13.5–14% PEG 2000 MME) and 1μL $TolC^{YFRS}$ protein (20 mg/mL in buffer B) was mixed with 1 μL reservoir (0.1 M Hepes pH 7.0, 15 mM KCl, 10 mM $MgCl_2$, 27.5% PEG 400, 0.1% DDM). Crystals grew to maximum size in 5 d at 23 °C before visibly deteriorating.

Data Collection, Processing, Structure Determination, and Analysis. Crystals were transferred incrementally into a final cryoprotectant containing 7% PEG 2000 MME, 10% PEG 200, and 15% PEG 400 ($TolC^{RS}$) or 30% PEG 400 ($TolC^{YFRS}$) and flash frozen in liquid nitrogen. X-ray diffraction data for $TolC^{RS}$ were collected at 100 K at beamline I02 of the Diamond Light Source (Didcot) using an ADSC Q315 CCD detector. $TolC^{YFRS}$ data were collected in-house on a Rigaku rotating anode (Cu radiation) with an R-AXIS IV detector system. Diffraction data for both crystals were processed in MOSFLM and scaled using SCALA in the CCP4 suite (23). Phases were determined using molecular replacement in PHASER ($TolC^{RS}$) or AMORE ($TolC^{YFRS}$), with $TolC^{WT}$ (PDB 1EK9) as the search model. Refinement of the $TolC^{YFRS}$ structure was initially performed in REFMAC5 followed, like the $TolC^{RS}$ structure, by simulated annealing in CNS 1.2 (24) and finally B-factor refinement in PHENIX 1.3 (25). Loose noncrystallographic symmetry restraints, between TolC monomers, were used over invariant (between the open-state and wild-type) parts of the structure. For both open-state structures, each round of refinement was followed by rounds of manual rebuilding in COOT (26). Geometries of the final refined models were analyzed with Rampage (27). A summary of the data collection and refinement statistics for both crystals is given in Table S1. As for $TolC^{WT}$, both models encompass residues 1–428. In regions of poor density, side chains have been left with high B-factors. Waters and PEG fragments were added where there was clear F_O-F_C and $2F_O$-F_C density (above 3σ and 1σ, respectively) and where the geometry was appropriate. TolC structures were aligned over the invariant sections (residues 20–100 and 225–320, i.e., the OM β-barrel and the α-helical coiled coil above the equatorial domain) using superpose in the CCP4 suite. Pore size area was calculated using the program HOLE (16). LSQMAN (28) was used to determine rmsd values. Figures were prepared using PyMol (29).

Docking Adaptor AcrA to the Advanced Open-State $TolC^{YFRS}$. The AcrA α-helical hairpin was docked to the previously defined binding site on $TolC^{YFRS}$ coiled coils, using established docking methods (11). The spherical polar Fourier-based surface and electrostatic complementarity search methods of Hex 5.1 (22) was used to locate a binding position on the $TolC^{YFRS}$ open-state structure that was closest (final backbone rmsd 4.5 Å) to that in the previous data-driven modeling of the pump (9). The starting AcrA model hairpin had a conformation relative to the contiguous lipoyl domain that was defined by previous cross-linking guided docking. For docking AcrB to $TolC^{YFRS}$ we have used an "open" AcrB model in which the β-strands of the DC domain have been made structurally similar to the DN domain (9). This has been used to visualize possible TolC interacting residues in the register established by that work.

ACKNOWLEDGMENTS. We thank the staff at Diamond Light Source for their help. We thank Elke Maier for expert technical assistance with conductance measurements. The work was supported by a Wellcome Trust Programme Grant (to V.K. and C.H.).

1. Koronakis V, Eswaran J, Hughes C (2004) Structure and function of TolC: The bacterial exit duct for proteins and drugs. *Annu Rev Biochem* 73:467–489.
2. Eswaran J, Koronakis E, Higgins MK, Hughes C, Koronakis V (2004) Three's company: Component structures bring a closer view of tripartite drug efflux pumps. *Curr Opin Struct Biol* 14:741–747.
3. Blair JM, Piddock LJ (2009) Structure, function and inhibition of RND efflux pumps in Gram-negative bacteria: An update. *Curr Opin Microbiol* 12:512–519.
4. Thanabalu T, Koronakis E, Hughes C, Koronakis V (1998) Substrate-induced assembly of a contiguous channel for protein export from E.coli: Reversible bridging of an inner-membrane translocase to an outer membrane exit pore. *EMBO J* 17:6487–6496.
5. Koronakis V, Sharff A, Koronakis E, Luisi B, Hughes C (2000) Crystal structure of the bacterial membrane protein TolC central to multidrug efflux and protein export. *Nature* 405:914–919.
6. Murakami S, Nakashima R, Yamashita E, Yamaguchi A (2002) Crystal structure of bacterial multidrug efflux transporter AcrB. *Nature* 419:587–593.
7. Yu EW, McDermott G, Zgurskaya HI, Nikaido H, Koshland DE, Jr. (2003) Structural basis of multiple drug-binding capacity of the AcrB multidrug efflux pump. *Science* 300:976–980.
8. Mikolosko J, Bobyk K, Zgurskaya HI, Ghosh P (2006) Conformational flexibility in the multidrug efflux system protein AcrA. *Structure* 14:577–587.
9. Symmons MF, Bokma E, Koronakis E, Hughes C, Koronakis V (2009) The assembled structure of a complete tripartite bacterial multidrug efflux pump. *Proc Natl Acad Sci USA* 106:7173–7178.
10. Higgins MK, Bokma E, Koronakis E, Hughes C, Koronakis V (2004) Structure of the periplasmic component of a bacterial drug efflux pump. *Proc Natl Acad Sci USA* 101: 9994–9999.
11. Lobedanz S, et al. (2007) A periplasmic coiled-coil interface underlying TolC recruitment and the assembly of bacterial drug efflux pumps. *Proc Natl Acad Sci USA* 104:4612–4617.
12. Tamura N, Murakami S, Oyama Y, Ishiguro M, Yamaguchi A (2005) Direct interaction of multidrug efflux transporter AcrB and outer membrane channel TolC detected via site-directed disulfide cross-linking. *Biochemistry* 44:11115–11121.
13. Touzé T, et al. (2004) Interactions underlying assembly of the Escherichia coli AcrAB-TolC multidrug efflux system. *Mol Microbiol* 53:697–706.
14. Andersen C, et al. (2002) Transition to the open state of the TolC periplasmic tunnel entrance. *Proc Natl Acad Sci USA* 99:11103–11108.
15. Eswaran J, Hughes C, Koronakis V (2003) Locking TolC entrance helices to prevent protein translocation by the bacterial type I export apparatus. *J Mol Biol* 327:309–315.
16. Smart OS, Goodfellow JM, Wallace BA (1993) The pore dimensions of gramicidin A. *Biophys J* 65:2455–2460.
17. Higgins MK, et al. (2004) Structure of the ligand-blocked periplasmic entrance of the bacterial multidrug efflux protein TolC. *J Mol Biol* 342:697–702.
18. Bavro VN, et al. (2008) Assembly and channel opening in a bacterial drug efflux machine. *Mol Cell* 30:114–121.
19. Murakami S, Nakashima R, Yamashita E, Matsumoto T, Yamaguchi A (2006) Crystal structures of a multidrug transporter reveal a functionally rotating mechanism. *Nature* 443:173–179.
20. Seeger MA, et al. (2006) Structural asymmetry of AcrB trimer suggests a peristaltic pump mechanism. *Science* 313:1295–1298.
21. Andersen C, Hughes C, Koronakis V (2002) Electrophysiological behavior of the TolC channel-tunnel in planar lipid bilayers. *J Membr Biol* 185:83–92.
22. Ritchie DW, Kozakov D, Vajda S (2008) Accelerating and focusing protein-protein docking correlations using multi-dimensional rotational FFT generating functions. *Bioinformatics* 24:1865–1873.
23. Collaborative Computational Project, Number 4 (1994) The CCP4 suite: Programs for protein crystallography. *Acta Crystallogr D Biol Crystallogr* 50:760–763.
24. Brünger AT, et al. (1998) Crystallography and NMR system: A new software suite for macromolecular structure determination. *Acta Crystallogr D Biol Crystallogr* 54:905–921.
25. Adams PD, et al. (2002) PHENIX: Building new software for automated crystallographic structure determination. *Acta Crystallogr D Biol Crystallogr* 58: 1948–1954.
26. Emsley P, Cowtan K (2004) Coot: Model-building tools for molecular graphics. *Acta Crystallogr D Biol Crystallogr* 60:2126–2132.
27. Lovell SC, et al. (2003) Structure validation by C alpha geometry: Phi, psi and C beta deviation. *Proteins: Struct Funct Genet* 50:437–450.
28. Kleywegt GJ (1999) Experimental assessment of differences between related protein crystal structures. *Acta Crystallogr D Biol Crystallogr* 55:1878–1884.
29. DeLano WL (2002) *The PyMol Molecular Graphics System* (DeLano Scientific, Palo Alto, CA).